Mathematical modeling of the self-pressurizing mechanism for microstructured fiber drawing

Christopher J. Voyce, Alistair D. Fitt, John R. Hayes, and Tanya M. Monro

***Abstract*— A method is proposed for modeling the self-pressurization of optical fibers that are sealed before drawing. The model is solved numerically and the results compared with experimental results. An explanation of the mechanism is presented and a numerical investigation is undertaken to optimize the choice of experimental parameters to minimize the transient effects of sealed preform drawing.**

***Index Terms*— Mathematical modeling, optical fiber, optical fiber applications, optical fiber fabrication, optical fiber theory, pressure effects.**

I. Introduction

MICROSTRUCTURED optical fibers (MOFs) are manufactured by heating a macroscopic structured preform (typically a few centimetres in diameter), and drawing it down to the required dimensions (typically 125μm in diameter). In the case of silica MOFs, preforms are often manufactured by stacking capillary tubes inside a larger capillary tubes, forming a hexagonal pattern of holes. The presence of air holes in the cross-section presents both challenges and opportunities for the fabrication of these fibers. Competition between viscosity and surface tension effects can alter the size and shape of the holes during the drawing process, and in extreme cases hole closure can occur.

The fabrication of structured preforms is one of the most labor intensive parts of the manufacturing process and it is often desirable to produce a number of different fiber profiles from a single preform by altering the conditions under which the fiber is drawn. For this reason predictive modeling capabilities are crucial, as is the ability to understand and control undesirable effects such as the change of hole-shapes and the closure of interstitial holes.

For many MOFs it is important to be able to collapse interstitial holes, and gaps between the outer (larger) capillary and the inner (smaller) capillaries. Since surface tension acts more on the inner capillaries than on the outer tube, the inner capillaries suffer a greater degree of collapse on drawing [1]. The collapse of interstitial holes can be achieved by pressurizing the inner capillaries, allowing the inner capillaries to be fitted to the outer tube, thus preserving the preform structure. Pressurizing the capillaries can be accomplished in two ways. Either an overpressure can be applied to the top of the preform, thus maintaining the holes at an elevated pressure [2], [3], or the tubes may be "sealed". Sealing is often the method of choice because it is more simple to execute experimentally and has been found to work surprisingly well. Unfortunately, when capillary tubes are sealed, the drawn fiber exhibits an inner-diameter that gradually changes with time. It is observed that the inner-radius gradually increases as the fiber is drawn before later decreasing. No significant change in the outer diameter is observed since conservation of mass requires that any change in outer diameter is an order of magnitude smaller than changes in the inner diameter. The effect is clearly due to a gradual increase and then decrease in the overpressure within the preform, but no attempt has previously been made to explain or model this effect.

There exist numerous studies of optical-fiber drawing, including studies related to the drawing of capillary tubes (see, for example, [2], [3], [4], [5], [6], [7]). In this paper we develop a model to describe the sealing process and predict the characteristics of the evolution in the fiber geometry during the draw. We compare predictions of the model with experimental results, and suggest a strategy for minimizing such pressure and geometry fluctuations.

The remainder of the paper is organized as follows: in §II we describe the experimental sealing process, in §II-A we detail the model assumptions, before describing the model in §III. We give experimental and numerical results in §IV and discussion the effects of one of the assumptions in §IV-B. In §V we suggest methods to improve the method of capillary sealing before concluding in §VI.

II. The sealing process

A capillary tube significantly longer than the furnace is sealed at one end, and placed in the furnace with the sealed end uppermost, leaving much of the preform protruding from the furnace (see Fig. 1). As the furnace temperature is increased to the "drop temperature" of the glass, the furnace and glass are in thermal equilibrium. However, the portion of tube protruding from the furnace is at a much lower temperature than the furnace. Conduction and radiation are both significant sources of heating and the temperature of the tube above the furnace is not precisely known, but is significantly higher than the ambient air as a result of radiative heating.

As the air in the capillary heats up and expands, an amount of air exits the system at the bottom of the furnace, since the bottom of the tube is still open to the atmosphere. The tube is then pulled as normal and thins rapidly, initially closing

Manuscript received January 20, 2002; revised November 18, 2002.

C.J. Voyce is with the Mathematical Institute, University of Oxford, U.K. (e-mail: voyce@maths.ox.ac.uk).

A.D. Fitt is head of the School of Mathematics, University of Southampton, U.K. (e-mail: adf@maths.soton.ac.uk).

J.R. Hayes is with the Optoelectronics Research Centre, University of Southampton, U.K. (e-mail: jrh@orc.soton.ac.uk).

T.M. Monro is Director of the Centre of Expertise in Photonics, University of Adelaide, Australia (e-mail: tanya.monro@adelaide.edu.au).

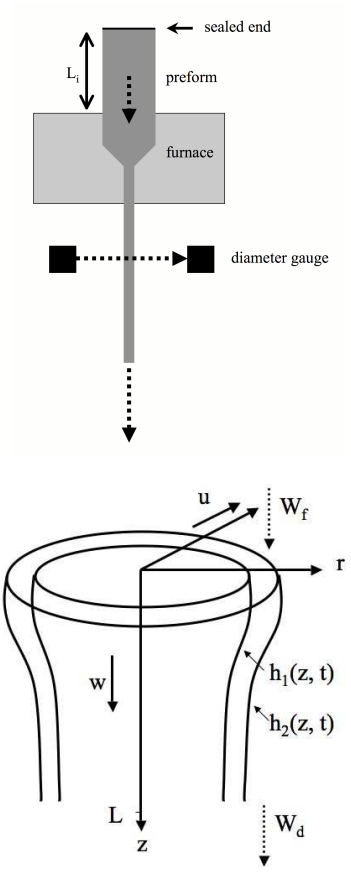

Fig. 1. (Upper) Schematic of experimental set-up. A capillary tube is sealed at the top, left open at the bottom, and passed slowly into the furnace. As the preform melts and is drawn, the tube initially closes under the action of surface tension. A quasi-steady state is the reached and the fiber is drawn. The capillary tube radius and pressure then slowly vary with time. (Lower) Problem geometry.

(at the bottom) under the effects of surface tension. This is a transient effect that is normally referred to as "the drop". A quasi-steady fiber diameter is then obtained. The volume of glass and gas lost from the tube by the initial part of the pull, which serves to close the hole, is not significant and will be assumed negligible.

The pull never reaches an exact steady-state (only a quasi-steady state, where we may ignore the time dependence in the governing equations and simply allow all dependent variables to depend on time) because air is being removed from the capillary tube at the end of the furnace, thus modifying the ratio of glass to air. Furthermore, as the fiber is drawn the capillary tube is lowered into the furnace, increasing the average temperature of the air in the tube. It will be shown that these effects combine to give a continually changing pressure inside the capillary tube, resulting in changes in fiber geometry.

A. Model assumptions

We assume that:

(1) the mass of glass and gas lost in the initial drop are negligible and may be ignored.
(2) the temperature of the glass is known for the large portion outside the furnace and the draw does not commence until thermal equilibrium is achieved.
(3) the air within the capillary tube is assumed to be in thermal equilibrium with the glass throughout.
(4) the temperature profile of the glass is assumed (a) to vary linearly with distance and (b) not to depend on time.
(5) whilst the temperature of the glass varies inside the furnace, the viscosity of the glass will be assumed constant in this region (including the correct variable viscosity introduces numerical difficulties but does not significantly alter the predictions).
(6) the effects of surface tension are negligible.

III. Modeling

A schematic diagram of the capillary geometry is shown in Fig. 1. To develop a mathematical model for the process of capillary drawing that is capable of including the effects of internal hole pressurization, surface tension, gravity and inertia as well as the effects of preform rotation we begin with the Navier-Stokes equations using cylindrical coordinates where the glass viscosity is assumed a function of both axial and radial position.

We non-dimensionalize the governing equations, and simplify them by taking advantage of the slender preform geometry. This allows the equations to be solved in closed-form in certain limiting cases (e.g. ignoring gravity, inertia and surface tension, see [7]). We apply the same simplifying approximations to the physical boundary conditions, before finally deriving a closed system of "leading-order" equations that describe the drawing of rotating preforms. The free parameters in the model include (i) the glass viscosity (determined by the glass properties and the furnace temperature profile), (ii) the surface tension, (iii) the length of the drawing furnace, iv) the initial preform geometry (i.e. inner and outer diameters), and v) the feeding and drawing speeds.

The final equations are given by

$$\rho(h_2^2 - h_1^2)(w_{0t} + w_0 w_{0z} - g) = \Big[3\mu(h_2^2 - h_1^2)w_{0z} + \gamma(h_1 + h_2) + \frac{\rho}{4}(h_2^4 - h_1^4)B^2\Big]_z, \tag{1}$$

$$(h_1^2)_t + (h_1^2 w_0)_z = \frac{h_1 h_2\left[2p_0 h_1 h_2 - 2\gamma(h_1 + h_2) + \rho h_1 h_2 B^2(h_2^2 - h_1^2)\right]}{2\mu(h_2^2 - h_1^2)}, \tag{2}$$

$$(h_2^2)_t + (h_2^2 w_0)_z = \frac{h_1 h_2\left[2p_0 h_1 h_2 - 2\gamma(h_1 + h_2) + \rho h_1 h_2 B^2(h_2^2 - h_1^2)\right]}{2\mu(h_2^2 - h_1^2)}, \tag{3}$$

TABLE I
NOTATION

Symbol	Definition
t	time
z	distance along capillary axis
r	distance perpendicular to axis
p	hole pressure
p_a	atmospheric pressure
p_0	hole overpressure (pressure over atmospheric)
g	acceleration due to gravity
ρ	density
R	ideal gas constant
μ	viscosity
γ	surface tension
L	furnace length
T	temperature
B	angular frequency
B_0	preform angular frequency
w_0	leading-order downstream fluid velocity
W_f	feeding speed for preform
W_d	drawing speed for fiber
h_2	outer radius
h_1	inner radius
h_{20}	initial outer preform radius
h_{10}	initial inner preform radius
β	$\log(W_d/W_f)$
L_i	length of preform above furnace at time $t=0$
z_{min}	length of preform above furnace at time t
T_{min}	temperature at the top of the capillary (estimated)
T_{max}	peak furnace temperature

$$\rho\left[h_2^2(h_2^2B)_t - h_1^2(h_1^2B)_t\right] + \rho w_0\left[h_2^2(h_2^2B)_z - h_1^2(h_1^2B)_z\right] + \frac{\rho}{\mu}p_0Bh_1^2h_2^2 - \frac{\rho\gamma Bh_1h_2}{\mu}(h_1+h_2) + \frac{\rho^2B^3h_1^2h_2^2}{2\mu}(h_2^2-h_1^2) = \mu\left[(h_2^4-h_1^4)B_z\right]_z. \tag{4}$$

and the boundary conditions are given by

$$h_1(0)=h_{10},\quad h_2(0)=h_{20},\quad w_0(0)=W_f,$$
$$w_0(L)=W_d,\quad B(0)=B_0,\quad B(L)=0, \tag{5}$$

where all notation is defined in Table I. Subscripts denote differentiation.

Equations (1)–(4) are a system of partial differential equations. The accompanying boundary conditions pose a two-point boundary value problem that must be solved numerically. We employ standard library routines by implementing the NAG routine D02HAF [8], which uses an efficient Runge-Kutta-Merson method. It is not our intention here to discuss the equations above, and instead refer the reader to Voyce *et al.* [7] for a full derivation and discussion. Equations (1)–(4) give an expression for h_1 in terms of p_0 that, together with the sealing model, will be used to predict the time dependence of p_0 and hence h_1.

Considering only the steady-state version of these equations and ignoring the effects of gravity, the inertial-force term and those of surface tension (see [3] and [7] for details of how this affects the solutions) and preform rotation, (1)–(4) become

$$\left[(h_2^2-h_1^2)w_{0z}\right]_z = 0, \tag{6}$$
$$(h_1^2w_0)_z = \frac{h_1^2h_2^2p_0}{\mu(h_2^2-h_1^2)}, \tag{7}$$
$$(h_2^2w_0)_z = \frac{h_1^2h_2^2p_0}{\mu(h_2^2-h_1^2)}, \tag{8}$$

and may be solved by eliminating $(h_2^2-h_1^2)$ and solving to give $w_0 = W_f e^{\beta z/L}$. We are then left with equations for h_2 and h_1. Since we are principally interested in the volume of air enclosed within the capillary it is helpful to know how h_1 varies with z as a function of overpressure, which is given by

$$h_1 = h_{10}\sqrt{\frac{(h_{20}^2-h_{10}^2)\exp\left(-\frac{\left(\mu\beta^2W_fze^{\beta z/L}+p_0L^2\right)e^{-\beta z/L}}{\mu\beta W_fL}\right)}{h_{20}^2\exp\left(-\frac{p_0L}{\mu\beta W_f}\right)-h_{10}^2\exp\left(-\frac{p_0Le^{-\beta z/L}}{\mu\beta W_f}\right)}}. \tag{9}$$

We assume a quasi-steady solution for h_1 by setting $p_0 = p_0(t)$ in (9) and calculate the variation in pressure with time as the preform is lowered into the furnace, before using (9) to predict the time-dependence of the fiber inner-radius.

A. Pressure calculation

The temperature $T(z)$ is considered known within the furnace [9] but must be estimated for the remainder of the capillary tube (the part that protrudes from the top of the furnace). The top of the capillary tube is located at $z=-L_i$ for $t=0$ and moves with speed W_f.

We assume that the air inside the capillary tube is an ideal gas obeying the ideal-gas law

$$p = \rho RT, \tag{10}$$

where R is the universal gas constant.

The total mass of air inside the capillary tube is given by

$$\int_{z_{min}}^{0}\pi h_{10}^2\,\rho(z,t)\;dz + \int_0^L \pi h_1^2(z,t)\rho(z,t)\;dz + \int_0^t \pi h_1^2(L,t')\,\rho(L,t')\,W_d\;dt', \tag{11}$$

where $z_{min} = -L_i + W_f t$ denotes the top of the capillary tube. The first term in (11) represents the mass of gas in the part of the preform above the furnace. The second term represents the mass of gas in the furnace. The third term accounts for the mass of gas that leaves the system and becomes trapped in the fiber. This is determined by the density of gas, the draw speed and the fiber radius at $z=L$.

Since the total mass of gas is constant we find, using (10), that

$$\frac{\partial}{\partial t}\left(\int_{z_{min}}^{0}\pi h_{10}^2\frac{p(t)}{RT(z)}\,dz+\int_{0}^{L}\pi h_1^2(z,t)\frac{p(t)}{RT(z)}\,dz\right)+\pi h_1^2(L,t)\,\frac{p(t)}{RT(L)}W_d=0, \tag{12}$$

which, on writing $p(t)=p_0(t)+p_a$ where p_a denotes atmospheric pressure, gives

$$\frac{\partial}{\partial t}\left[h_{10}^2\int_{z_{min}}^{0}\frac{(p_0(t)+p_a)}{T(z)}\,dz+\int_{0}^{L}\frac{h_1^2(z,t)(p_0(t)+p_a)}{T(z)}\,dz\right]+h_1^2(L,t)\,\frac{(p_0(t)+p_a)}{T(L)}W_d=0. \tag{13}$$

Substituting in the expression (9) for $h_1(z,t)$ gives an equation for $p_0(t)$. Once $p_0(t)$ is determined, (9) may be used to determine the manner in which $h_1(L,t)$ varies with time. Since (9) was obtained by solving (1)–(5) and assuming a steady-state process, the methodology employed here assumes that the timescales in (1)–(4) are much smaller than than the timescale for the change of $p_0(t)$ and $h_1(L,t)$ in (13); equivalent to a quasi-steady analysis.

An inspection of (13) reveals that the second term will always be much smaller than the first because $T(z'')>T(z')$ where $z_{min}<z'<0$ and $0<z''<L$, and $h_1(z)/h_{10}\ll 1$ when $0<z\leq L$. Furthermore, since $|z_{min}|$ is always much smaller than L (the capillary tube is never quite pushed fully into the furnace in practice), we may ignore the second term since it is always at least a factor of $L/|z_{min}|\ll 1$ smaller than the first. This leaves an equation for p_0 given by

$$h_{10}^2\frac{\partial}{\partial t}\int_{z_{min}}^{0}\frac{(p_0(t)+p_a)}{T(z)}\,dz+h_1^2(L,t)\,\frac{(p_0(t)+p_a)}{T(L)}W_d=0. \tag{14}$$

The function $T(z)$ is assumed to be given by

$$T(z)=T_{max}-\frac{(T_{min}-T_{max})z}{L_i}, \tag{15}$$

where T_{min} and T_{max} are the temperature at the top of the capillary tube at the start of the experiment and the peak furnace temperature respectively. Finally, we assume that the viscosity of Suprasil F300 glass [6] is given by

$$\mu=5.8\times 10^{-8}\exp\left(\frac{515400}{8.3145(T_{max}-273)+2271.10567}\right),$$

where T_{max} is now given in units of C and the viscosity is expressed in units of Poise.

When (15) is used in (14) and the resulting equation simplified, we arrive at a first-order non-linear ordinary differential equation for $p_0(t)$ that must be solved numerically. Having determined $p_0(t)$, $h_1(L,t)$ may be calculated from (9).

IV. Comparison with experiment

Experiments were conducted at the Optoelectronics Research Centre, University of Southampton, U.K. We directly compare the results of an experiment with numerical predictions made by the model. The experiments described below used silica glass, but the methodology and analysis is applicable to all glasses.

The initial dimensions of the capillary tube were chosen so that the effects of surface tension could be minimized (i.e. a large h_{10} and h_{20} were chosen). A temperature distribution for the glass was determined by assuming a linear profile and $T_{min}=1460$C. The preform extended above the furnace with $L_i=0.8m$. Other experimental parameters were $h_{10}=0.95$cm, $h_{20}=1.25$cm, $W_f=1.5$mm/minute, $W_d=15$m/minute and $T_{max}=1840$C. The capillary was fed into the furnace at the prescribed speed, and the pressure and fiber geometry were continually monitored by sampling the fiber at regular intervals of time.

Numerical simulations that calculate $p_0(t)$ from (14) were performed using the parameter values given above. From this data (9) was used to compute the inner radius $h_1(L,t)$.

Numerical and experimental results for both $h_1(t)$ and $p_0(t)$ are shown in Figs. 2 and 3. In both cases a spline fit has been applied to the data. Given the fact that the temperature distribution of the capillary tube outside of the furnace has been crudely estimated, the temperature distribution in the furnace was assumed linear, and that the effects of surface tension have been ignored in this model, the qualitative agreement between experimental and numerical results is good. The form of both the pressure curve and the inner fiber-radius curve have the required shape: a more detailed examination of Figs. 2 and 3 is presented in §IV-A.

A. Explanation of the success of sealing

Controlling hole size or preventing hole closure through hole pressurization may be accomplished either by directly applying an overpressure or by sealing the preform before drawing. The sealing method is often chosen since experimentalists observe that it "automatically" prevents hole closure and maintains hole sizes whereas the direct application of an overpressure is sensitive to the pressure applied [3].

The model developed in this paper provides a possible explanation of this observation. The rate at which the pressure

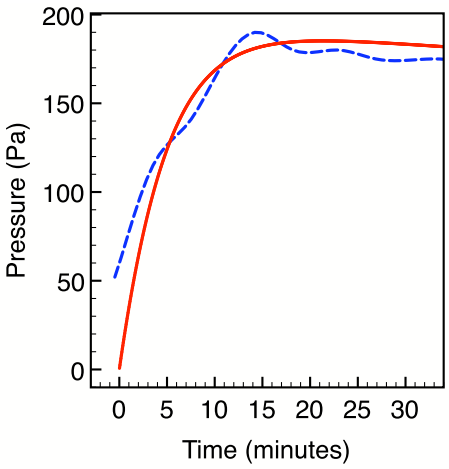

Fig. 2. Graphs to show the experimental (broken line) and numerical (solid line) results for $p_0(t)$. (Parameter values: $W_f = 2.5 \times 10^{-5}$, $W_d = 2.5 \times 10^{-1}$, $h_{20} = 1.25 \times 10^{-2}$, $h_{10} = 9.50 \times 10^{-3}$, $L_i = 8 \times 10^{-1}$, $T_{min} = 1460$, $T_{max} = 1840$. S.I. units are assumed.)

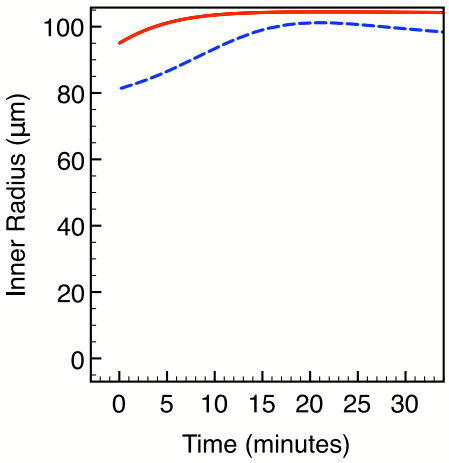

Fig. 3. Graphs to show the experimental (broken line) and numerical (solid line) results for $h_1(L,t)$. (Parameter values: $W_f = 2.5 \times 10^{-5}$, $W_d = 2.5 \times 10^{-1}$, $h_{20} = 1.25 \times 10^{-2}$, $h_{10} = 9.50 \times 10^{-3}$, $L_i = 8 \times 10^{-1}$, $T_{min} = 1460$, $T_{max} = 1840$. S.I. units are assumed.)

increases as the fiber is drawn depends on a balance of two effects. (i) As the preform is lowered into the furnace, the gas within heats up, thus increasing the overpressure. (ii) As the fiber is drawn, gas leaving the system at the bottom of the furnace becomes trapped in the fiber, which has the effect of counteracting the effect of the mechanism (i) and reducing the preform overpressure. To give an illustrative example of the feedback mechanism, suppose that surface tension were to completely close the hole (this does not happen in practice precisely because of this feedback mechanism). Glass (but no air) would leave the furnace at $z = L$. As the preform is gradually lowered into the furnace, the volume of air within the furnace region would remain constant and its average temperature would increase, whilst the volume of glass would decrease (the length of the tube decreases). Consequently the overpressure would increase until it was large enough to overcome the effects of surface tension at $z = L$. At this point the hole would reopen and equilibrium would eventually be established between hole size and overpressure.

The shape of the curves in Figs. 2 and 3 may therefore be interpreted in the following way: at the start of the drawing process much of the preform is above the furnace and at a lower temperature than the furnace. As the fiber is drawn and the preform is lowered into the furnace, the dominant effect is that of an increased average temperature for the air inside the preform, giving rise to both an increased overpressure and an increased fiber radius (see (9)). However as time proceeds the increase in average temperature per unit length of preform lowered into the furnace reduces. This allows the effect of air removal at $z = L$ to dominate, and the pressure thus begins to decrease, as does the fiber radius.

If the mechanism described above is correct, then as the feed speed is decreased to zero one would expect that the increase in pressure obtained through sealing would be significantly reduced (see upper graph of Fig. 4) and that as the feed speed is increased to large values the pressure inside the preform rises dramatically (see lower graph of Fig. 4).

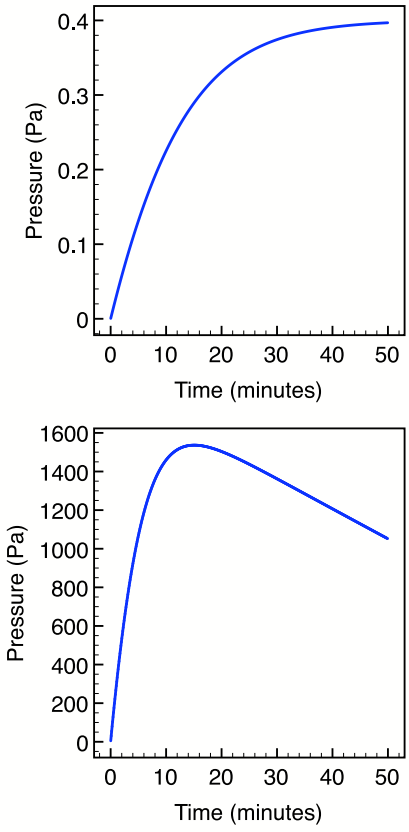

Fig. 4. Graphs to show effect of extremes in feed speed on the numerical solutions for $p_0(t)$, where $W_f = 1.67 \times 10^{-8}$ (upper) and $W_f = 1.67 \times 10^{-4}$ (lower). (Other parameter values: $W_d = 2.5 \times 10^{-1}$, $h_{20} = 1.25 \times 10^{-2}$, $h_{10} = 9.50 \times 10^{-3}$, $L_i = 8 \times 10^{-1}$, $T_{min} = 1200$, $T_{max} = 1840$. S.I. units are assumed.)

B. The effects of surface tension

As currently posed, the model neglects the effects of surface tension. Including surface tension in the model and performing a regular perturbation in γ gives (see [6])

$$\left(\frac{h_2^2(L)-h_1^2(L)}{h_1^2(L)}\right)=\left\{\frac{h_{20}e^{-\frac{\beta}{2}}+\psi}{h_{10}e^{-\frac{\beta}{2}}+\psi}\right\}^2-1, \tag{16}$$

where ψ is given by

$$\psi=\frac{\gamma L e^{-\beta}\left[(3h_{10}-h_{20})\left(1-e^{\frac{\beta}{2}}\right)+h_{10}e^{\frac{\beta}{2}}\left(e^{-\frac{\beta}{2}}-1\right)\right]}{3\beta W_f(h_{20}^2-h_{10}^2)}.$$

Thus, when surface tension is ignored we have

$$\left(\frac{h_2^2(L)-h_1^2(L)}{h_1^2(L)}\right)=\frac{h_{20}^2-h_{10}^2}{h_{10}^2}. \tag{17}$$

If the difference between (16) where surface tension is included and (17) (where $\gamma=0$) is greater than zero, less mass will leave when surface tension effects are accounted for, and vice versa. Consequently the hole overpressure is expected to be larger at any given time when the effects of surface tension are included if

$$\left(\frac{h_2^2(L)-h_1^2(L)}{h_1^2(L)}\right)-\frac{h_{20}^2-h_{10}^2}{h_{10}^2}>0, \tag{18}$$

or equivalently when

$$\frac{h_{20}e^{-\frac{\beta}{2}}+\frac{\gamma L e^{-\beta}\left[(3h_{10}-h_{20})\left(1-e^{\frac{\beta}{2}}\right)+h_{10}e^{\frac{\beta}{2}}\left(e^{-\frac{\beta}{2}}-1\right)\right]}{3\beta W_f(h_{20}^2-h_{10}^2)}}{h_{10}e^{-\frac{\beta}{2}}+\frac{\gamma L e^{-\beta}\left[(3h_{20}-h_{20})\left(1-e^{\frac{\beta}{2}}\right)+h_{10}e^{\frac{\beta}{2}}\left(e^{-\frac{\beta}{2}}-1\right)\right]}{3\beta W_f(h_{20}^2-h_{10}^2)}}>0. \tag{19}$$

Setting $W_f=1.5$mm/minute, $W_d=15$m/minute, $h_{20}=1.25$cm, $h_{10}=0.95$cm and using the given viscosity law and temperature distribution, (19) gives a value of 0.04. This suggests that we should expect to observe a larger pressure and smaller value of $h_1(L)$ than our model predicts. This is not observed experimentally and therefore the effects of surface tension do not seem to account for the difference between model predictions and experimental results.

Since it has already been shown that fiber geometry is particularly sensitive to the temperature profile of the glass [9], the most likely cause of the discrepancy between experimental and numerical results in an inadequate knowledge of the glass temperature profile, both within and outside of the furnace. We further note that the temperature profile of the preform outside the furnace may change as the preform is lowered into the furnace and heat transfer processes are modified. It is possible that a steady-state draw process was not achieved for the early part of the experiment. Additionally, it is possible that as the glass in the drawn fiber cools and the overpressure in the fiber decreases, the induced pressure gradient is sufficient to increase the rate at which air is removed from the preform-furnace system, thus decreasing the steady-state pressure in the preform and the fiber radius at $z=L$.

V. Optimization

We now investigate how best to prescribe experimental parameters in order to maximize the "flat" portion of the curves in Fig. 2, thus minimizing the time-fluctuations in fiber geometry.

Numerical simulations confirm that there is more than one way to flatten the (e.g. pressure) curve, such that a more stable fiber geometry results for a longer time. Increasing the length of the capillary protruding from the furnace (increasing L_i) flattens the pressure curve and vica versa. This can be seen by comparing the graphs of Fig. 5. A similar effect may also be accomplished by increasing the temperature of the top of the capillary, as can be seen by comparing the solid lines of Figs. 5 and 6. The explanation of these effects is that increasing the length of the capillary tube allows any increase or decrease in volume fraction of air in the capillary to be averaged over a greater volume, thus reducing the effect on the pressure. Similarly, by decreasing the difference in temperature between the top of the capillary and the furnace, the expansion of gas that occurs as the preform is lowered into the furnace is reduced and the transient effect on the pressure is therefore minimized. We therefore suggest that reducing the temperature gradient in the capillary and/or increasing the length of capillary used will produce a more stable fiber geometry in MOF manufacture. We note that increasing the temperature is likely to be the most practical solution since preform material is expensive, and increasing the length of the preform has the disadvantage of increasing the rise-time to reach maximal pressure, as seen in Fig. 5. Finally, we note that in the extreme case where the temperature at $z=-L_i$ is lowered significantly, the pressure may increase dramatically (Fig. 7, solid line) and when the temperature is increased to a temperature higher than the furnace temperature, the pressure (above atmospheric) in the preform actually becomes negative (Fig. 7, broken line).

VI. Conclusion

A model was developed to describe the time-fluctuating pressure and fiber geometry observed when sealed capillary tubes are drawn to fiber form. Numerical solutions to the equations compared favorably with experimental data, especially given the large uncertainties in quantities such as the temperature profile of the preform above the furnace. It is anticipated that once the uncertainties in experimental quantities are reduced, this model will provide an accurate tool for developing a method to control the size of extremely

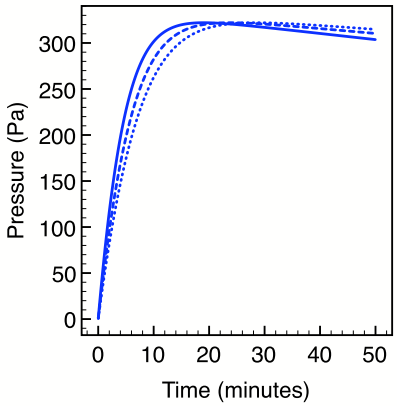

Fig. 5. Graph to show numerical solutions designed to minimize $p_{0t}(t)$ and $h_{1t}(L,t)$ where $L_i = 8 \times 10^{-1}$ (solid line), $L_i = 1$ (broken line) and $L_i = 1.2$ (dotted line). (Other parameter values: $W_f = 2.5 \times 10^{-5}$, $W_d = 2.5{\times}10^{-1}$, $h_{20} = 1.25{\times}10^{-2}$, $h_{10} = 9.50{\times}10^{-3}$, $T_{min} = 1200$, $T_{max} = 1840$. S.I. units are assumed.)

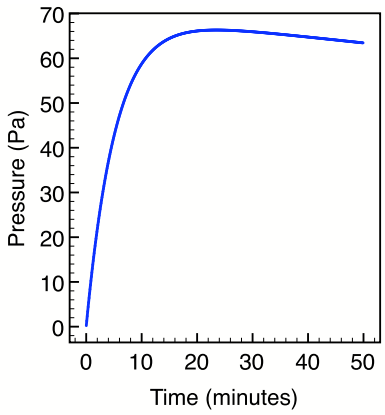

Fig. 6. Graph to show numerical solutions designed to minimize $p_{0t}(t)$ and $h_{1t}(L,t)$ where $T_{min} = 1700$. (Other parameter values: $W_f = 2.5{\times}10^{-5}$, $W_d = 2.5{\times}10^{-1}$, $h_{20} = 1.25{\times}10^{-2}$, $h_{10} = 9.50{\times}10^{-3}$, $L_i = 8{\times}10^{-1}$, $T_{max} = 1840$. S.I. units are assumed.)

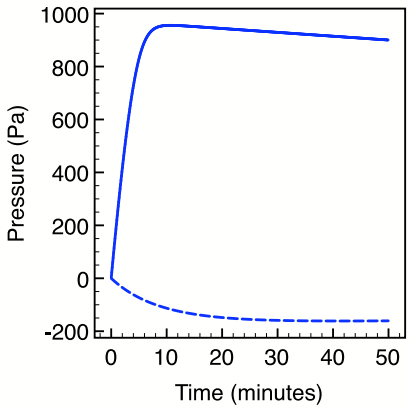

Fig. 7. Graph to show the effect of extremes in minimum temperature on the numerical solutions for $p_0(t)$, where $T_{min} = 200$ (solid line) and $T_{min} = 2200$ (broken line). (Other parameter values: $W_f = 2.5 \times 10^{-5}$, $W_d = 2.5{\times}10^{-1}$, $h_{20} = 1.25{\times}10^{-2}$, $h_{10} = 9.50{\times}10^{-3}$, $L_i = 8{\times}10^{-1}$, $T_{max} = 1840$. S.I. units are assumed.)

small holes (as a result of the feedback mechanism between hole size and hole overpressure).

A numerical study of the model suggestions that increasing the length of the capillary and/or increasing the temperature of the top of the capillary will assist in minimizing the time-fluctuations of fiber geometry.

The model may be extended to include the possibility of multiple holes (i.e. for MOFs). However, the effects of overpressure on holes in an MOF will surely depend on the position of the hole in the preform as well as its size. The model presented in this paper should be applicable to the holes towards the outer edge of an MOF preform, where the holes are expected to behave more independently than those closer to the center.

REFERENCES

[1] K. Furusawa, "Development of rare-earth doped microstructured optical fibres." Ph.D. dissertation, Optoelectronics Research Centre, University of Southampton, Southampton, SO17 1BJ, U.K., 2003.

[2] A. D. Fitt, K. Furusawa, T. M. Monro, and C. P. Please, "Modeling the fabrication of hollow fibers: capillary drawing." *Journal of Lightwave Technology*, vol. 19, no. 12, pp. 1924–31, 2001.

[3] A. D. Fitt, K. Furusawa, T. M. Monro, C. P. Please, and D. J. Richardson, "The mathematical modelling of capillary drawing for holey fibre manufacture." *Journal of Engineering Mathematics*, vol. 43, no. 2–4, pp. 201–227, 2002.

[4] C. J. Voyce, A. D. Fitt, and T. M. Monro, "Mathematical modelling of the drawing of spun capillary tubes." in *Progress in Industrial Mathematics at ECMI 2002*, A. Buikis, R. Ciegis, and A. D. Fitt, Eds. Berlin: Springer-Verlag, 2004, pp. 387–391.

[5] ——, "Mathematical model of the spinning of microstructured fibres." *Optics Express*, vol. 12, no. 23, pp. 5810–5820, 2004.

[6] C. J. Voyce, "The mathematical modelling of microstructured optical fibres." Ph.D. dissertation, School of Mathematics, University of Southampton, Southampton, SO17 1BJ, U.K., 2005.

[7] C. J. Voyce, A. D. Fitt, and T. M. Monro, "The mathematical modelling of rotating capillary tubes for holey-fibre manufacture." *Journal of Engineering Mathematics*, Accepted January 2007.

[8] http://gams.nist.gov/serve.cgi/Module/NAG/D02HAF/681/, "Module documentation for the numerical algorithms group (nag), limited, routine d02haf."

[9] C. J. Voyce, A. D. Fitt, and T. M. Monro, "Mathematical modeling as an accurate predictive tool in capillary and microstructured fibre manufacture: the effects of preform rotation." *Journal of Lightwave Technology*, Submitted 2007.

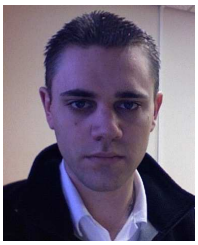

Christopher Voyce received his Ph.D. degree from the University of Southampton, U.K. before moving to the University of Adelaide, Australia. He is now at the Mathematical Institute, University of Oxford, U.K. His research interests lie in industrial applied mathematics.

Alistair Fitt received his D. Phil. degree from the University of Oxford, U.K. in 1983 for his work on the film cooling of turbine blades. He is currently Head of the School of Mathematics at the University of Southampton, U.K. Most of his mathematical career has been spent considering the mathematical modeling of industrial processes. He has also been a frequent contributor to Study Groups with Industry in many different worldwide locations. His other mathematical interests include the study of fluid and solid mechanics in human eyes, and various aspects of betting and gaming.

John Hayes joined the Optoelectronics Research Centre (ORC) at the University of Southampton, U.K. in 2003 as Senior Experimental Officer, working in the holey fiber group. Since then he has created a diverse range of novel structures including a square core jacketed air clad fiber and fibers with sub-wavelength holes. Prior to joining the ORC he worked in industrial process development and technology transfer roles, and headed a team of engineers supporting high volume optical fiber manufacture.

Tanya Monro has been the Chair of Photonics and the Director of the Centre of Expertise in Photonics within the School of Chemistry & Physics at the University of Adelaide since 2005. From 1998 to 2004, Tanya worked at the ORC at the University of Southampton, U.K. on silica and soft glass MOFs. Prior to this she completed a Ph.D. at the University of Sydney, Australia on self-written waveguides in photosensitive glasses. Her current research within the Centre of Expertise in Photonics focuses on the design, fabrication and device applications of new classes of soft glass MOFs, including work on new transmission fibers, highly nonlinear fibers, chem/bio sensing with new fibers and novel fiber lasers.